An experimental evaluation of regular polyhedron loudspeakers as omnidirectional sources of sound

Timothy W. Leishman,[a] Sarah Rollins, and Heather M. Smith
Acoustics Research Group, Department of Physics and Astronomy, Eyring Science Center, Brigham Young University, Provo, Utah 84602

(Received 12 December 2005; revised 15 June 2006; accepted 15 June 2006)

Multiple-driver dodecahedron loudspeakers are commonly used in room acoustics measurements as omnidirectional sources of sound. Yet they and other regular polyhedron loudspeakers become "multidirectional" above their omnidirectional cutoff frequencies (often near 1 kHz). Because these cutoff frequencies normally fall within common measurement bandwidths, one might question whether anything is really extraordinary about the dodecahedron loudspeaker or whether another regular polyhedron geometry would actually produce better average omnidirectionality over these bandwidths. This paper explores these questions through measured data, analysis, and comparison of frequency-dependent directivities of several regular polyhedron loudspeaker prototypes. It provides insights into their radiation properties and introduces an alternative method of quantifying omnidirectionality: the area-weighted spatial standard deviation of radiated levels over a free-field measurement sphere. It compares this method to the ISO 3382:1997(E) standard method, revealing certain discrepancies between the two approaches. A dodecahedron loudspeaker is shown to produce a relatively high cutoff frequency and reasonable radiation uniformity over measurement bandwidths. However, it does not necessarily excel as a better omnidirectional source than other regular polyhedron loudspeakers. A tetrahedron loudspeaker with an equal midradius provides the best average radiation uniformity over a 4 kHz bandwidth, even though it exhibits the lowest cutoff frequency. [DOI: 10.1121/1.2221552]

PACS number(s): 43.55.Mc, 43.38.Ja, 43.38.Hz, 43.20.Rz [NX] Pages: 1411–1422

I. INTRODUCTION

In an effort to employ consistent omnidirectional sources in room acoustics measurements, acousticians have long resorted to multiple-driver loudspeakers based on regular polyhedra or platonic solid enclosure geometries. Regular polyhedron loudspeakers (RPLs) typically incorporate small in-phase direct-radiator drivers of consistent manufacture, mounted centrally in the faces of their sealed enclosures. One international standard suggests that their acceptance, particularly that of the dodecahedron loudspeaker, has become nearly universal.[1]

Despite the predominance of the dodecahedron loudspeaker, several important questions should be addressed. First, is anything really extraordinary about the dodecahedron loudspeaker—especially when its radiation is considered over *entire* measurement bandwidths? Second, how do directional characteristics of loudspeakers based on other platonic solid geometries compare to those based on the dodecahedron geometry over these same bandwidths? Third, is it possible that other platonic solid geometries actually provide better omnidirectional radiation when averaged over the bandwidths? This paper will respond to these questions to enhance understanding and implementation of the sources as measurement tools.

A regular polyhedron is a convex polyhedron composed of identical regular polygonal faces (equal side lengths and vertex angles). The five regular polyhedra are the tetrahedron (4 faces), hexahedron or cube (6 faces), octahedron (8 faces), dodecahedron (12 faces), and icosahedron (20 faces).[2] If an RPL is geometrically centered at the origin of the spherical coordinate system, its normal facial axes are distributed uniformly throughout the combined angular coordinates. However, despite their geometric uniformities and symmetries, RPLs are known to exhibit undesirable directional behaviors (i.e., nonspherical radiation patterns) above frequencies that may be termed omnidirectional "cutoff frequencies." Several factors contribute to the frequency-dependent departure from the omnidirectional ideal. They include interference between radiation from discrete drivers, inherent directivities of individual drivers, and diffraction effects.

An omnidirectional acoustic source is ideal for many applications because it radiates sound *equally* in *all* directions. A *unidirectional* source radiates sound predominantly in only *one* direction. A *multidirectional* source may be defined as one radiating sound predominantly in *several* directions, between the extremes of an omnidirectional source and a unidirectional source. Over large portions of common measurement bandwidths, RPLs are typically multidirectional sources.

In a previous study of RPLs, Tarnow used spherical harmonic expansions, group representation theory, and several source idealizations to computationally characterize low- to mid-frequency radiation and omnidirectional cutoff frequencies.[3,4] In his work, he found that cutoff frequencies should progressively increase for higher-order polyhedra with fixed effective enclosure radii. Close inspection of his work also suggests another important point: if an enclosure is

[a]Electronic mail: tim_leishman@byu.edu

reasonably sized to accommodate drivers with adequate low-frequency response and sound power output, the omnidirectional cutoff frequencies regularly fall within bandwidths of common room acoustics measurements. For example, his results suggest that a dodecahedron loudspeaker with an effective radius a begins to exhibit significant directivity above $ka=3$, where k is the acoustic wave number. For a common dodecahedron loudspeaker designed to balance omnidirectionality with desired sound power output, the effective radius typically places the omnidirectional cutoff frequency in the vicinity of 1 kHz. While this cutoff frequency can be increased by using smaller loudspeaker drivers and enclosures, low-frequency response and sound power output will generally suffer as a result. In a recent development, Witew and Behler employed multiple sources in a multiway configuration to maintain sufficient broadband omnidirectionality and sound power output for room acoustic parameter measurements.[5]

Recognition of undesirable directional behavior of RPLs is also apparent in established standards for room acoustics measurements.[1,6] They allow qualification of presumably omnidirectional sources through spatial averaging of free-field radiation over measurement arcs in a single plane and spectral averaging over proportional frequency bands. They also relax omnidirectional requirements at higher frequencies and ignore directional behavior above 5.6 kHz. One standard requires source rotations through three angular positions and averaging of subsequent measurement results when source directivity is found to significantly affect measured room acoustic parameters.[6] Nevertheless, none of these concessions changes the fact that presumably omnidirectional sources exhibit unprescribed and undesirable directivities at many frequencies of interest.

The authors have undertaken a research effort to further characterize RPL radiation through analysis and comparison of the frequency-dependent directivities of several RPLs over common measurement bandwidths. This paper focuses on key experimental findings of that effort. Two sets of RPLs were constructed with specific geometric properties to enable equitable comparisons. The first consisted of RPLs with equal midradii (EM). [The midradius of a regular polyhedron is the distance from its geometrical center to the midpoint of any edge (facial side).] The second consisted of RPLs with equal volume (EV) allocation per loudspeaker driver, resulting in progressively larger total enclosure volumes for higher-order polyhedra. While sources with other dimensions or geometries might also have been studied (including those of various RPLs with consistent spacing between adjacent loudspeaker drivers), the results presented here reveal several important trends. Special measurement and data processing tools were developed specifically for the effort. An alternative method of quantifying source omnidirectionlity was developed and compared to the current standard method found in ISO 3382:1997(E).[6] It involved an area-weighted spatial standard deviation of radiated levels evaluated over a free-field measurement sphere.

The following section discusses the experimental procedures. The subsequent sections present results and analysis, then compare the two methods of quantifying source omnidirectionality. The final section presents conclusions from the study and several suggestions for further work.

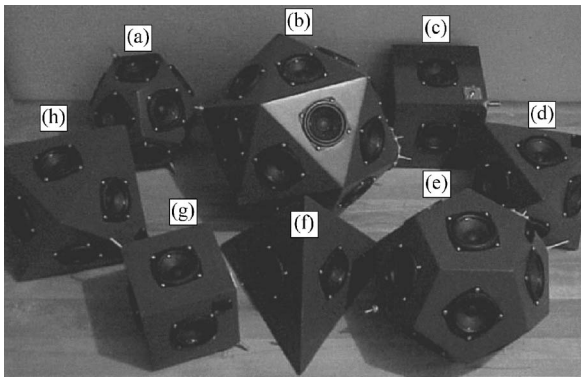

FIG. 1. Equal midradii (EM) and equal volume per driver (EV) RPLs. (a) EM dodecahedron. (b) EV icosahedron. (c) EV hexahedron. (d) EM octahedron. (e) EV dodecahedron. (f) EM/EV tetrahedron. (g) EM hexahedron. (h) EV octahedron.

II. EXPERIMENTAL PROCEDURES

Geometric properties of regular polyhedra, including their midradii and volumes, are often expressed in terms of edge or facial side lengths.[7,8] Established relationships were used to design and construct the eight RPLs shown in Fig. 1 with the properties listed in Table I. The loudspeakers consisted of one EM and one EV RPL for each polyhedron type, except the tetrahedron and icosahedron. A single tetrahedron loudspeaker was constructed to simultaneously satisfy both the EM and EV criteria. Only one EV icosahedron loudspeaker was constructed because the Aura NS3-194-8D drivers selected for the RPLs (with nominal 80 mm diameters) would not fit within a compact icosahedron satisfying the EM criterion. As indicated in Table I, the EM value was chosen to be 11.0 cm while the EV value (external enclosure volume per driver) was chosen to be 887.4 cm^3. The sealed enclosures were constructed of 1.9-cm-thick birch plywood. Approximately half of their sealed air volumes were filled with acoustically absorptive fibrous material. All RPLs were wired for equal in-phase signal to each driver and an overall nominal impedance between 4 and 8 Ω.

As suggested in Fig. 2, the radiated fields were measured by mounting each RPL on a narrow stand in an anechoic

TABLE I. External geometric properties for the eight experimental RPLs. The equal midradius (EM) value was chosen to be 11.0 cm while the equal volume per driver (EV) value was chosen to be 887.4 cm^3.

RPL	Edge length (cm)	Midradius (cm)	Volume per driver (cm^3)	Total volume (cm^3)
EM/EV tetrahedron	31.1	11.0	887.4	3 549
EM hexahedron	15.6	11.0	627.4	3 764
EM octahedron	22.0	11.0	627.4	5 020
EM dodecahedron	8.4	11.0	378.9	4 547
EV hexahedron	17.5	12.3	887.4	5 325
EV octahedron	24.7	12.3	887.4	7 099
EV dodecahedron	11.2	14.6	887.4	10 648
EV icosahedron	20.1	16.3	887.4	17 748

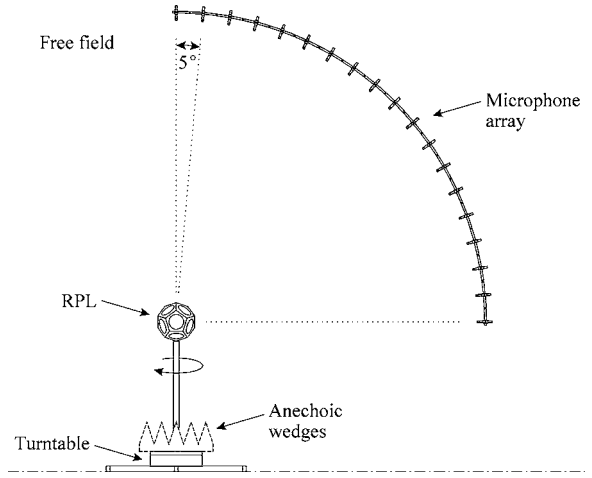

FIG. 2. Diagram of the experimental setup in an anechoic chamber. A dodecahedron is shown mounted on the turntable stand. The turntable is covered with wedges to maintain anechoic conditions. A 90° arc array of microphones senses the radiated field.

chamber, then rotating it under a quarter-circle microphone array with a computer-controlled turntable. Thick absorptive wedges were positioned on top of the turntable to reduce its reflection and scattering. The turntable was controlled to rotate in $\Delta\phi=5°$steps, producing measurement dependence in the azimuthal angle ϕ. Nineteen Larson Davis 2551 microphones (type 1 free-field electrets) were connected to The Modal Shop TMS426C01 preamplifiers and radially oriented in the 90° measurement arc. The arc had a 2.1 m radius and was positioned in the first quadrant of the vertical plane above the RPL. The axis of the top microphone $(\theta=0°)$ was directed along a vertical line running through the RPL center. The axis of the bottom microphone $(\theta=90°)$ was directed along a horizontal line running through the center. The curved array incorporated uniform $\Delta\theta=5°$ angular increments between adjacent microphones, enabling the same sampling in the polar angle as in the azimuthal angle. To obtain a full sphere of measured data, it was necessary to measure the top radiation hemisphere, turn the RPL upside down, align it, then measure the bottom hemisphere.

The microphones were individually calibrated at 1 kHz and connected to a multichannel dynamic signal analyzer based on Hewlett-Packard E1432A VXI cards. Their sensitivities were entered into the Data Physics DP620 control software and periodically checked for drift. The analyzer also provided a broadband pseudorandom excitation signal to drive the RPLs through a power amplifier. Frequency response and coherence functions between the excitation signal and the microphone outputs were generated between 0 and 20 kHz with 1600 uniform frequency bins (12.5 Hz bandwidths). The analyzer was configured to take 30 stable averages for each measurement. Frequency response functions were considered a good choice for the directivity measurements because they provided smooth frequency dependence in the measured data and many postprocessing options.

For each source rotation position in ϕ, the 19 frequency response functions in θ were automatically exported for postprocessing. The measurement set was repeated with each 5° turntable increment until the RPL had been rotated through a full 360°. Once both hemispheres were measured, a composite 2664-point set of complex frequency response functions was compiled to enable thorough characterization of the RPL radiation.

Observation of the frequency response and coherence data suggested that the low-frequency roll off of the RPLs was approximately 100 Hz. The anechoic cutoff frequency of the chamber was somewhat lower than 100 Hz. Nevertheless, those low-frequency limitations were inconsequential for the directivity measurements because all RPLs displayed consistent omnidirectional radiation near this spectral region.

III. MEASUREMENT RESULTS

To produce graphical representation of the RPL directivity patterns, normalized frequency response function levels were first determined using the formula

$$L_{m,n}(f) = 20 \log\left[\frac{|H_{m,n}(f)|}{|H_{m,n}(f)|_{\max}}\right], \tag{1}$$

where $|H_{m,n}(f)|$ is the modulus of the complex frequency response function at the point m,n on the measurement sphere and $|H_{m,n}(f)|_{\max}$ is the maximum of all $|H_{m,n}(f)|$ for the given frequency f. The indices m and n are integer multipliers of the 5° increments in θ and ϕ, respectively. Thus, $\theta_m=m\Delta\theta$, where $m=0,1,2,\ldots,M-1$, and $M=37$ is the number of measurement positions in θ. Similarly, $\phi_n=n\Delta\phi$, where $n=0,1,2,\ldots,N-1$, and $N=72$ is the number of measurement positions in ϕ. The levels were plotted for all RPLs at several frequencies to produce narrowband (12.5 Hz bandwidth) directivity balloons.

Animations of the balloons over frequency provided interesting insights into their frequency-dependent evolutions. As anticipated, the RPLs all produced nearly omnidirectional fields (spherical balloon plots) below about 1 kHz. However, their directivity patterns differed dramatically above this frequency. Figures 3 and 4 show the narrowband plots for the eight RPLs at 2 and 4 kHz, respectively, revealing several distinct lobe patterns and symmetries. Several factors contributed to the directivity patterns. For any given RPL and frequency, an individual loudspeaker driver has a radiation pattern that depends upon its cone diameter, other geometric features, and specific vibrational characteristics. It also depends upon the surrounding enclosure and diffraction effects. When all drivers are in simultaneous operation, the complex pressure produced by each and every driver superposes to generate the composite field and associated directivity pattern. Constructive and destructive interference is affected by the individual driver directivities, spacings, and angular orientations. Since the drivers are not perfectly matched, the pattern symmetries may not be ideally related to the associated polyhedron symmetries.

The presence of the lobes, which do not necessarily correspond to driver axes at these frequencies, demonstrate significant departure from the omnidirectional ideal. At 2 kHz, the larger EV RPLs appear to be more advanced in their multidirectional behaviors than their smaller EM RPL coun-

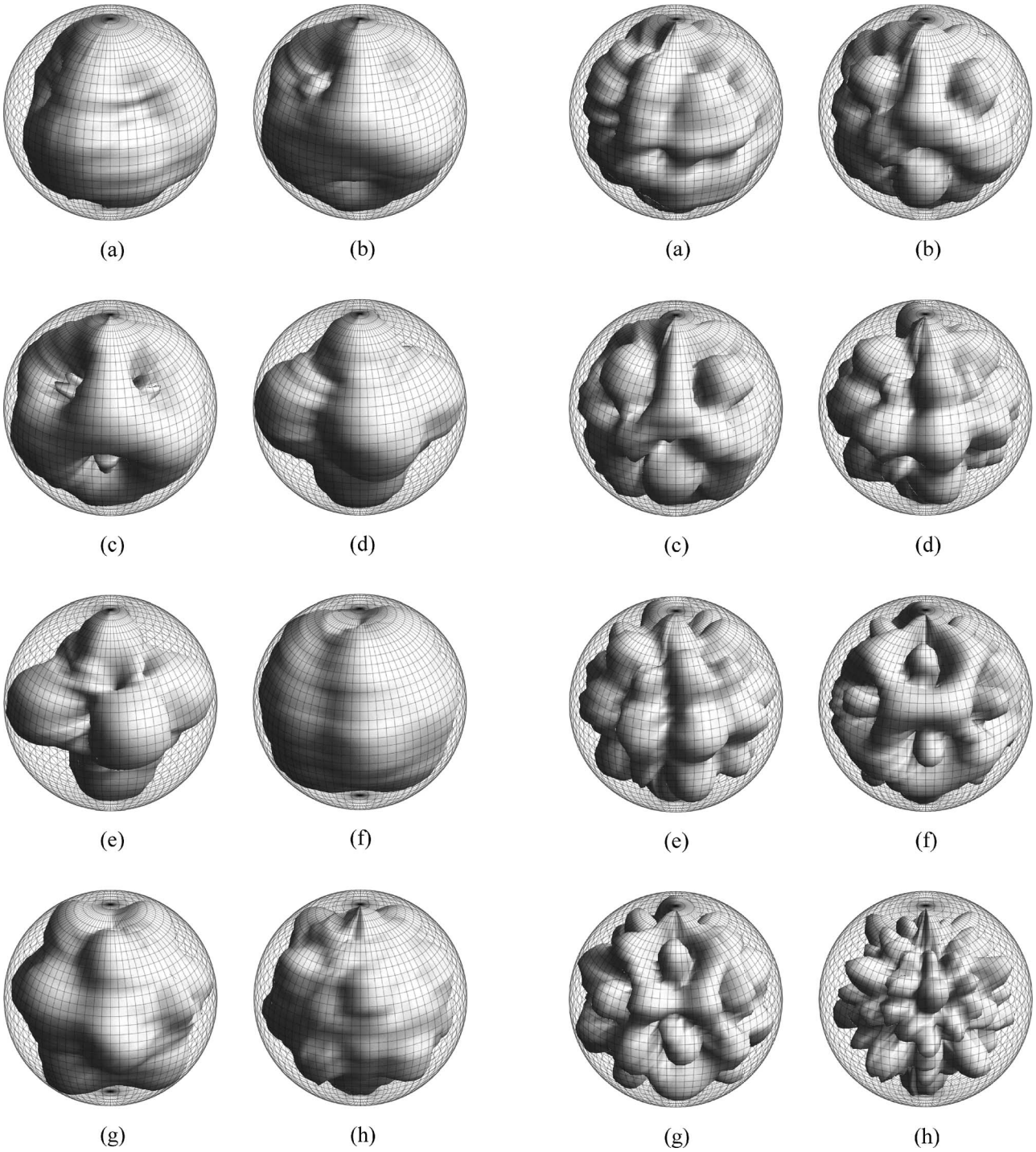

FIG. 3. Narrowband directivity balloon plots for all eight RPLs operating at 2 kHz. (a) EM/EV tetrahedron. (b) EM hexahedron. (c) EV hexahedron. (d) EM octahedron. (e) EV octahedron. (f) EM dodecahedron. (g) EV dodecahedron. (h) EV icosahedron. As shown in the plots, lobes become apparent above 1 kHz, providing clear evidence of departure from omnidirectional radiation. The surfaces of the superposed mesh spheres represent uniform normalized values of 0 dB. The origin represents a value of −20 dB, meaning that the mesh sphere radii are 20 dB.

FIG. 4. Narrowband directivity balloon plots for all eight RPLs operating at 4 kHz. (a) EM/EV tetrahedron. (b) EM hexahedron. (c) EV hexahedron. (d) EM octahedron. (e) EV octahedron. (f) EM dodecahedron. (g) EV dodecahedron. (h) EV icosahedron. The distinct lobes at this frequency generally demonstrate further departure from omnidirectional radiation. The radii of the superposed mesh spheres again represent 20 dB.

terparts. Interestingly, the tetrahedron loudspeaker appears to show greater omnidirectionality at both frequencies than several of the higher-order RPLs.

When considered over full-octave and third-octave proportional bands, the directivity balloons had patterns similar to the narrowband balloons, but with expected smoothing that increased substantially for larger bandwidths. From this observation alone, it is clear that one should exercise caution in using broad proportional-band measurements to characterize source directivity at higher frequencies.

IV. ANALYSIS

To consolidate the measurement results and improve understanding of the frequency-dependent RPL directivities,

the data was further analyzed using two methods: the ISO 3382 source qualification method, and an area-weighted spatial standard deviation method. Additional statistical analyses also provided insights for establishing RPL omnidirectionality.

A. ISO 3382

To regulate the impact of source directivity on room acoustics measurements, standards often state that excitation sources should be as omnidirectional as possible—with deviations from perfect omnidirectionality arising only within prescribed limits.[1,6] The source qualification procedure outlined in ISO 3382 is representative of those found in other standards. It requires that a source be driven with octave bands of pink noise to produce radiated free-field sound pressures. The pressure for each band is measured at a minimum radial distance of 1.5 m and averaged over 30° measurement arcs. These 30° "gliding" averages are then referenced to a 360° energetic average in the measurement plane to compute a "directional deviation" in decibels. The directional deviation must remain within maximum allowable limits to satisfy the qualification criteria. Because the standard specifically allows 5° field measurement increments to compute the averages, it is well suited to the data measured in this work.

Two types of filters were applied to the measured frequency response functions as postprocessing options. One was designed to equalize the RPLs for flat sound power response. The other was designed to weight either the equalized or unequalized responses as though the RPLs were driven by a pink noise signal. Since the standard suggests pink noise excitation and octave-band sound pressure level measurements without mention of equalization, the squared moduli of the weighted narrowband frequency response functions were first summed into base-2 octave bands[9] without sound power equalization. The directional deviation in each octave band was then calculated as the worst-case difference between various energetic gliding averages (six neighboring values in 30° arcs) of the equatorial measurement plane ($\theta_{18}=90°$) and the energetic average of all values in a full 360° circle of the same plane. Sound power equalization and pink-noise weighting were subsequently found to produce only small changes to the frequency-dependent curves.

The directional deviations for the EM and EV RPLs are plotted in Figs. 5 and 6, along with the maximum ISO 3382 deviation limits. The two lines shown for each RPL represent the largest positive and negative 30° arc deviations from the 360° energetic average. Such figures are commonly published by omnidirectional source manufacturers to demonstrate compliance with ISO standards and allow potential users to draw conclusions about their source directivities.

According to Fig. 5, all EM RPLs demonstrated nearly ideal omnidirectional radiation characteristics through the 500 Hz octave band. The tetrahedron loudspeaker was the first to depart from minimal deviation values beginning in the 1 kHz octave band. All other sources departed in the 2 kHz octave band. In that band, the hexahedron appears to be the most omnidirectional source, followed by the dodecahedron, the tetrahedron, then the octahedron. In the 4 kHz octave band, the octahedron appears to be the most omnidirectional source, followed by the tetrahedron, the hexahedron, then the dodecahedron. In the 8 kHz octave band, the hexahedron and octahedron appear to perform best, while the tetrahedron and dodecahedron appear to perform worst. These rankings are summarized in Table II, along with comparative rankings to be discussed later. Based on these results, the hexahedron appears to be the most omnidirectional EM RPL over the measurement bandwidth.

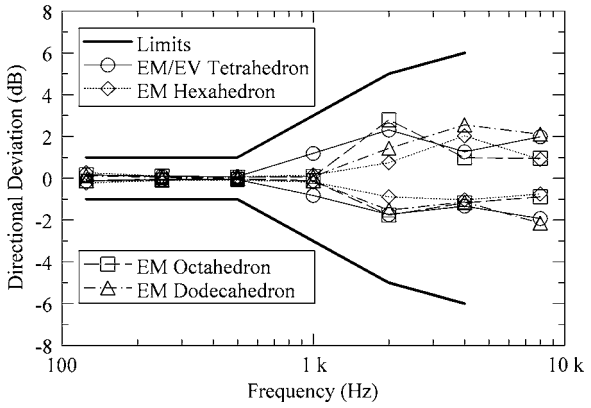

FIG. 5. Octave-band directional deviations for the EM RPLs based on an implementation of the ISO 3382 source qualification procedure. The extreme positive and negative deviation curves are plotted along with the maximum ISO 3382 deviation limits.

For the EV RPL results presented in Fig. 6, we again find the tetrahedron to be the first to depart from minimal deviation values in the 1 kHz octave band. Rankings for higher octave bands are summarized in Table II. From these results, the icosahedron appears to be the most omnidirectional EV RPL over the measurement bandwidth.

Given such comparative assertions, one may be justified in asking whether the data represented in the graphs is truly sufficient to establish omnidirectionality or to form a solid basis for rankings. A better approach would involve a more comprehensive understanding of the radiated fields and a pertinent summary of their characteristics.

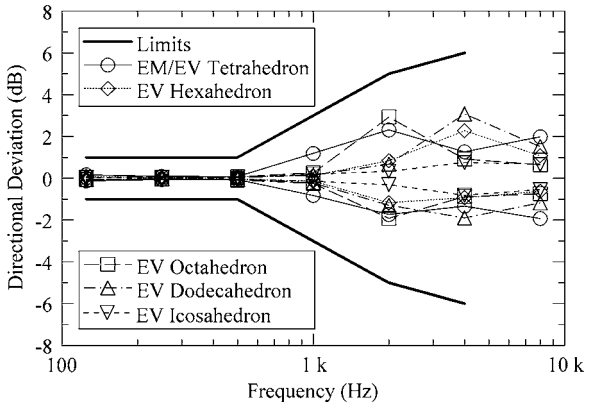

FIG. 6. Octave-band directional deviations for the EV RPLs based on an implementation of the ISO 3382 source qualification procedure. The extreme positive and negative deviation curves are plotted along with the maximum ISO 3382 deviation limits.

TABLE II. Approximate EM and EV RPL performance rankings for the 2, 4, and 8 kHz octave bands, according to results from the ISO 3382 and spatial standard deviation methods. Overall rankings are also given as composite rankings from the three octave bands.

	ISO 3382 method				Standard deviation method			
RPL	2 kHz	4 kHz	8 kHz	Overall	2 kHz	4 kHz	8 kHz	Overall
EM/EV tetrahedron	3	2	3–4	3	2	1	4	2
EM hexahedron	1	3	1–2	1	3	3	3	3
EM octahedron	4	1	1–2	2	4	4	2	4
EM dodecahedron	2	4	3–4	4	1	2	1	1
EM/EV tetrahedron	4	3	5	5	3	1	5	3–4
EM hexahedron	3	4	1–3	2	4	2	3	3–4
EV octahedron	5	1–2	1–3	3	5	4	4	5
EV dodecahedron	2	5	4	4	1	5	1–2	2
EV icosahedron	1	1–2	1–3	1	2	3	1–2	1

B. Area-weighted spatial standard deviation of levels

In the search for other means to characterize RPL directivity, an area-weighted spatial standard deviation was calculated from each complete set of 2664 narrowband measurements. Several standard deviation formulas (e.g., energetic, arithmetic level, unweighted, area-weighted, etc.) were explored to determine which provided results corresponding best to observed directional behaviors. Because the standard deviation should be zero for perfect omnidirectional radiation, it should be consistently small for all measured RPLs below 1 kHz to agree with observations. At any frequency above 1 kHz, it should agree (from a qualitative standpoint) with visualizations of the RPL balloon plots.

While an energetic standard deviation formulation was found to be useful and physically appropriate, another formulation was also found to favorably characterize the observations. It was the area-weighted spatial standard deviation of either normalized or unnormalized frequency response function levels,

$$\sigma_{\mathrm{AWL}}(f)=\sqrt{\frac{\sum_{m=0}^{M-1}\sum_{n=0}^{N-1}S_{m,n}[L_{m,n}(f)-\langle L_{m,n}(f)\rangle_S]^2}{\sum_{m=0}^{M-1}\sum_{n=0}^{N-1}S_{m,n}}},\quad(2)$$

where the arithmetic area-weighted spatial average of levels is given by

$$\langle L_{m,n}(f)\rangle_S=\frac{\sum_{m=0}^{M-1}\sum_{n=0}^{N-1}S_{m,n}L_{m,n}(f)}{\sum_{m=0}^{M-1}\sum_{n=0}^{N-1}S_{m,n}}.\quad(3)$$

The factor $S_{m,n}$ in these equations is the area weighting factor (i.e., the effective sampling area per microphone on the measurement sphere of radius $r=2.1$ m), determined by surface integration over appropriate sections of the measurement sphere:

$$S_{m,n}=\int_{\phi_n-\Delta\phi/2}^{\phi_n+\Delta\phi/2}\int_0^{\Delta\theta/2}r^2\sin(\theta)d\theta d\phi$$
$$=2r^2\Delta\phi\sin^2\left(\frac{\Delta\theta}{4}\right)=\frac{4\pi r^2}{N}\sin^2\left(\frac{\Delta\theta}{4}\right),\quad m=0,\quad(4)$$

$$S_{m,n}\int_{\phi_n-\Delta\phi/2}^{\phi_n+\Delta\phi/2}\int_{\theta_m-\Delta\theta/2}^{\theta_m+\Delta\theta/2}r^2\sin(\theta)d\theta d\phi$$
$$=2r^2\Delta\phi\sin(\theta_m)\sin\left(\frac{\Delta\theta}{2}\right),\quad 1\leqslant m\leqslant 35,\quad(5)$$

$$S_{m,n}\int_{\phi_n-\Delta\phi/2}^{\phi_n+\Delta\phi/2}\int_{\pi-\Delta\theta/2}^{\pi}r^2\sin(\theta)d\theta d\phi$$
$$=2r^2\Delta\phi\sin^2\left(\frac{\Delta\theta}{4}\right)=\frac{4\pi r^2}{N}\sin^2\left(\frac{\Delta\theta}{4}\right),\quad m=36.\quad(6)$$

These definitions are consistent for all values of n (see Fig. 7). The sampling areas of the two poles have been segmented into N equal pie slices for convenience in the summations. As formulated, the standard deviation is an asymptotically unbiased estimator, but for a finite number of samples, it has a small downward bias. No assumption is made about a normal distribution of the levels.

Interestingly, this approach is similar to approaches mentioned by Schroeder,[10] D'Antonio,[11] Cox,[12] and Hargreaves *et al.*[13,14] for evaluating the effectiveness of diffusing surfaces. The primary difference here is that radiated pressures are being measured rather than scattered pressures. Cox and Hargreaves *et al.* argued in favor of using levels in such formulas because they form a better "linear perceptual scale" for listeners and those visually evaluating decibel plots. They also suggested that an energetic spatially averaged level could be used in place of Eq. (3). However, this modification only produced a maximum positive correction of around 0.2 dB in the narrowband standard deviations well above the omnidirectional cutoff frequencies. Since the RPLs radiated fields with "moderate to good" uniformity at all frequencies of interest, the arithmetic spatial average in Eq. (3) was considered adequate to rank their performances.

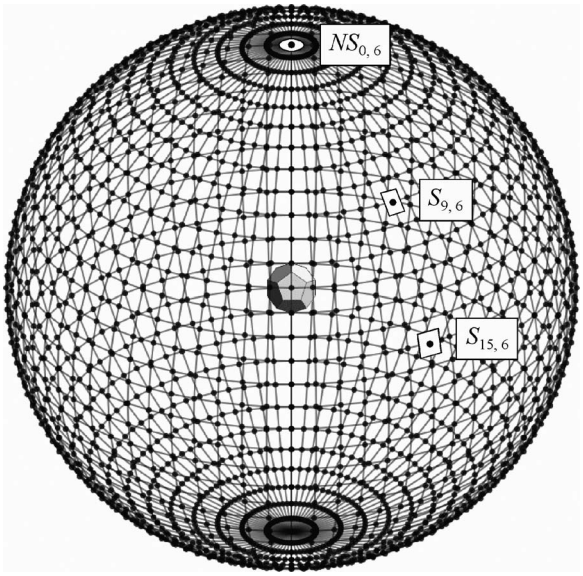

FIG. 7. A representation of sampling points (microphone positions) on the measurement sphere. The effective sampling area for each point differs, as suggested by the sampling areas $NS_{0,6}$, $S_{9,6}$, and $S_{15,6}$. The sampling areas of the two poles are segmented into N equal pie slices of areas $S_{0,n}$ and $S_{36,n}$ for convenience in the summations. The total polar sampling areas are then $NS_{0,n}$ and $NS_{36,n}$.

The resulting narrowband standard deviation plots are given in Figs. 8 and 9. They confirm that the RPLs did depart from omnidirectional behavior at cutoff frequencies in the vicinity of 1 kHz, then exhibited varying degrees of directivity above those frequencies. (Rising standard deviation values below 150 Hz are caused by poor measurement coherence and may be ignored.) Table III shows the cutoff frequencies for the RPLs, determined as the frequencies above which the standard deviations consistently exceeded an arbitrary threshold of 0.5 dB (shown by the dotted horizontal lines in Figs. 8 and 9). These frequencies are consistently but not dramatically higher than the conservative estimates given by Tarnow.[3,4] To compensate for the prediction offset and to better address expected cutoff orders, the next two columns of the table show ratios of measured cutoff frequencies for each RPL to the EM/EV tetrahedron cutoff

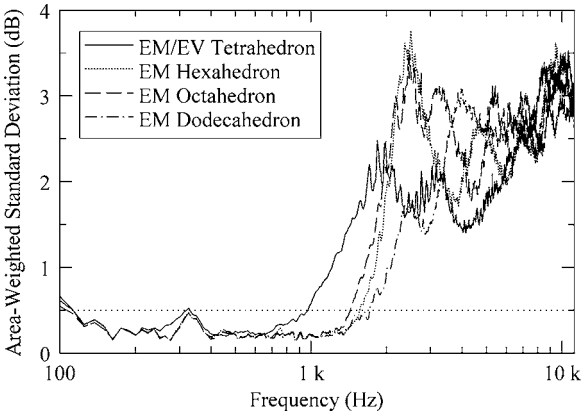

FIG. 8. Narrowband area-weighed spatial standard deviations for the EM RPLs. The omnidirectional cutoff frequency for each RPL is determined as the frequency above which the standard deviation consistently exceeds an arbitrary threshold of 0.5 dB (shown by the horizontal dotted line).

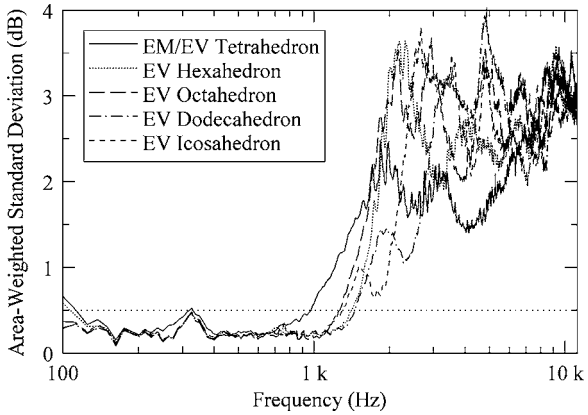

FIG. 9. Narrowband area-weighted spatial standard deviations for the EV RPLs. The omnidirectional cutoff frequency for each RPL is determined as the frequency above which the standard deviation consistently exceeds an arbitrary threshold of 0.5 dB (shown by the horizontal dotted line).

frequency, and similar approximate cutoff frequency ratios based on Tarnow's work. (The latter assume that a constructed RPL midradius can be substituted directly for Tarnow's "mean radius" a.) In the next two columns, the table provides the applicable EM/EV cutoff frequency ratios for each RPL shape and a comparative radius ratio with respect to the EM/EV tetrahedron midradius (which is equivalent to all EM RPL midradii). This radius ratio is used in the last column to adjust the measured cutoff frequency ratios from the second column and thus enable rough evaluation of relative EV RPL cutoff frequencies caused more by their shapes than their midradii. The EV and EM values for similar shapes in this column are generally closer than those in the second column. Of course, since the loudspeaker drivers were not scaled for the larger EV RPLs, one would not expect ideal agreement. Other properties may also come into play.

From low frequency to high frequency, the cutoff order for the four EM RPLs was (1) tetrahedron, (2) octahedron, (3) hexahedron, and (4) dodecahedron, almost agreeing with Tarnow's order. Because the cutoff frequency of the octahedron comes before its polyhedron order would suggest, one might initially surmise that its geometry is somehow less desirable than expected. However, comparison of the measured and Tarnow cutoff frequency ratios in Table III suggests that the hexahedron geometry is actually more desirable than expected. Of course, other factors must also be considered. The dodecahedron loudspeaker produced a relative cutoff frequency that was lower than expected. While the tetrahedron loudspeaker produced the lowest of all cutoff frequencies (as expected), many of its higher-frequency standard deviation values were notably lower than those of the other RPLs. In fact, as shown in Fig. 8, it clearly produced the most omnidirectional characteristics in a range extending from approximately 3 to 6 kHz, agreeing with the balloon plot observations mentioned in Sec. III.

The cutoff order for the five EV RPLs was (1) tetrahedron, (2) octahedron, (3) icosahedron, (4) hexahedron, and (5) dodecahedron. In this case, the cutoff orders of both the octahedron and icosahedron came before their polyhedron orders would suggest. However, for this set, the higher-order

TABLE III. Measured cutoff frequencies and related values for the eight RPLs. The cutoff frequencies f_c were defined as those above which the narrowband spatial standard deviations consistently exceeded a threshold of 0.5 dB. Ratios of the various frequencies to that of the EM/EV tetrahedron ($f_{c,t}$) are given, along with similar approximate ratios derived from Tarnow's work (Refs. 3 and 4). Ratios of cutoff frequencies for similar EM and EV RPL shapes are also given as $f_{c,\mathrm{EM}}/f_{c,\mathrm{EV}}$, followed by comparative radius ratios a/a_t and radius-adjusted cutoff frequency ratios $f_c/f_{c,t}\times a/a_t$.

RPL	Measured cutoff frequency f_c (Hz)	Measured cutoff ratio $f_c/f_{c,t}$	Tarnow cutoff ratio $f_c/f_{c,t}$	EM/EV cutoff ratio $f_{c,\mathrm{EM}}/f_{c,\mathrm{EV}}$	Radius Ratio a/a_t	Adjusted measured cutoff ratio $f_c/f_{c,t}\times a/a_t$
EM/EV tetrahedron	975	1.00	1.0	1.00	1.00	1.00
EM hexahedron	1562.5	1.60	1.2	1.11	1.00	1.60
EM octahedron	1437.5	1.47	1.4	1.14	1.00	1.47
EM dodecahedron	1712.5	1.76	2.2	1.17	1.00	1.76
EV hexahedron	1412.5	1.49	1.0	1.11	1.12	1.67
EV octahedron	1262.5	1.29	1.3	1.14	1.12	1.44
EV dodecahedron	1462.5	1.50	1.6	1.17	1.33	2.00
EV icosahedron	1300	1.33	1.5	N/A	1.48	1.97

polyhedra had progressively larger midradii that could have impacted the sequence. Figures 8 and 9 clearly show that the larger EV hexahedron, octahedron, and dodecahedron loudspeakers had consistently lower cutoff frequencies than their smaller EM counterparts. Nevertheless, even after the cutoff frequency ratios were adjusted by radius ratios in the last column of Table III, other geometric features seemed to persist as significant determinants of the order. In fact, with the exception of the newly introduced icosahedron, the adjusted cutoff order was identical to that found for the EM RPLs. Comparison of the measured and Tarnow cutoff frequency ratios in Table III again reveals that the EV hexahedron ratio is higher than expected, while those of the EV dodecahedron and EV icosahedron are lower than expected.

The standard deviation formulation was also applied to the octave-band levels calculated from the pink-noise-weighted frequency response functions discussed in Sec. IV A (without prior sound power equalization). This enabled observation of broad standard deviation trends and a more equitable comparison to the results of the ISO 3382 qualification method. Progressively increasing octave bandwidths again produced sufficient spectral averaging to effectively decrease the spatial variation of the radiated fields at higher frequencies and therefore decrease the standard deviation values. Sound power equalization and pink-noise weighting were again found to produce only small changes to standard deviation curves derived from unfiltered octave-band data.

A careful comparison of the octave-band standard deviation curves revealed both agreement and disagreement with the results of the ISO 3382 method given in Figs. 5 and 6. For the EM RPLs, the tetrahedron was the first to depart from nearly ideal omnidirectional behavior in the 1 kHz octave band. In the 2 kHz octave band, the dodecahedron produced the most uniform radiation, followed by the tetrahedron and hexahedron, then finally the octahedron. In the 4 kHz octave band, the tetrahedron performed best, followed by the dodecahedron, the hexahedron, then the octahedron. In the 8 kHz octave band, the dodecahedron performed best, followed by the octahedron, the hexahedron, then the tetrahedron. These rankings are summarized in Table II for comparison with the rankings from the ISO 3382 method. Overall, the octave-band standard deviation curves suggested that the dodecahedron maintained the most uniform radiation while the octahedron maintained the worst. This observation agrees with the mean standard deviation results discussed in Sec. IV C 1 and given in Table IV.

For the EV RPLs, the tetrahedron was again the first to depart from its omnidirectional behavior. Rankings for higher octave bands are summarized in Table II. Overall, it appeared that the icosahedron maintained the best radiation uniformity over the octave bands while the octahedron maintained the worst. However, the performance ranking for the icosahedron does not agree well with the mean standard deviation ranking given in Table IV.

Some of the most prominent points of disagreement between the ISO curves in Figs. 5 and 6, and the octave-band standard deviation curves can be found through inspection of

TABLE IV. Frequency-averaged standard deviation for the eight RPLs. This figure of merit was calculated by taking the arithmetic average of the narrowband spatial standard deviation values through the 4 and 8 kHz octave bands. Rankings for the lowest average values are given separately for the EM and EV RPLs in each range.

	100 Hz to 5.6 kHz (through 4 kHz octave)		100 Hz to 11.2 kHz (through 8 kHz octave)	
RPL	$\langle\sigma(f)\rangle_f$ (dB)	Rank	$\langle\sigma(f)\rangle_f$ (dB)	Rank
EM/EV tetrahedron	1.48	1	2.17	2
EM hexahedron	1.75	3	2.27	3
EM octahedron	1.89	4	2.37	4
EM dodecahedron	1.59	2	2.16	1
EM average	1.68	N/A	2.24	N/A
EM/EV tetrahedron	1.48	1	2.17	1
EM hexahedron	1.88	2	2.34	3
EV octahedron	2.12	5	2.53	5
EV dodecahedron	1.95	3	2.32	2
EV icosahedron	1.98	4	2.35	4
EV average	1.88	N/A	2.34	N/A

Table II. They include dramatically different orders of omnidirectional performance rankings for the two octahedrons in the 4 kHz octave band and the two dodecahedrons in the 8 kHz octave band. They also include opposite overall performance rankings for the EM dodecahedron. Furthermore, only the standard deviation method confirms the visual observation that the tetrahedron displays the greatest uniformity in the 4 kHz octave band. Other less significant discrepancies become apparent through closer inspection of the table and figures.

C. Additional statistical properties

Even with the useful data reduction provided by frequency-dependent line graphs and octave-band analysis, additional reduction was desirable to more readily compare the omnidirectionality of the sources. While no assumption was made about normal distributions, basic statistical properties of the frequency-dependent spatial standard deviation functions could be useful for this purpose. These properties might even be used to produce single-number figures of merit.

1. Mean value

The frequency-averaged standard deviation $\langle \sigma(f) \rangle_f$ was the first property considered as a figure of merit. As shown in Table IV, it was calculated for each RPL as an average of the frequency-dependent standard deviation functions given by Eq. (2) for all narrowband frequencies within two averaging bandwidths. The first bandwidth was from 100 Hz to 5.6 kHz (i.e., through the 4 kHz octave band) and the second was from 100 Hz to 11.2 kHz (i.e., through the 8 kHz octave band). Lower values were expected to correspond more closely (on average) to ideal omnidirectional radiation patterns over the bandwidths. According to this approach, the EM/EV tetrahedron was found to be the most omnidirectional source over the 4 kHz bandwidth—even though it had the lowest cutoff frequency. The EM dodecahedron loudspeaker ran a close second in this bandwidth and performed best over the 8 kHz bandwidth. The EM/EV tetrahedron performed second best over the 8 kHz bandwidth and was consistently better than any EV RPL over either bandwidth. The EM hexahedron, octahedron, and dodecahedron loudspeakers performed consistently better than their larger EV counterparts. Unfortunately, it was found (as suggested by Cox in relationship to diffusing surfaces[15]) that a simple average of the standard deviations over a measurement bandwidth allowed good omnidirectional spectral regions to unduly compensate for poor spectral regions. A simple average also failed to represent other undesirable swings in directional behavior.

2. Notched box-whisker diagrams

A more thorough approach to the problem involves the creation and observation of notched box-whisker diagrams. These provide an excellent overview of directional behavior over frequency, without necessarily producing a single-number figure of merit. Such diagrams are typically used to summarize several statistical properties of data sets, enabling an observer to assess whether their distributions are skewed, or if outliers or irregular data values are present. In this case, they are used to summarize the distribution and grouping of the frequency-dependent spatial standard deviation values. Figures 10 and 11 show the diagrams for each EM RPL through the 4 and 8 kHz octave bands, respectively.

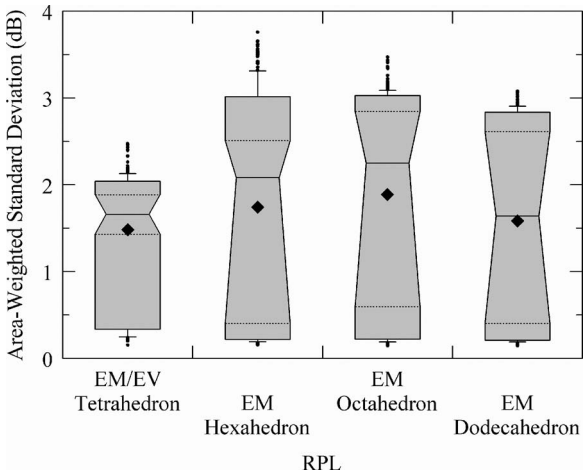

FIG. 10. Notched box-whisker diagrams showing the distribution and grouping of frequency-dependent spatial standard deviation values for the EM RPLs from 100 Hz to 5.6 kHz (through the 4 kHz octave band).

For a given RPL and measurement bandwidth, an individual notched box-whisker diagram is interpreted as follows. The median, or 50th percentile, is represented by a solid horizontal line at the narrowest point of the notched region. This line divides the diagram into upper and lower portions. The 25th and 75th percentiles are marked by dotted horizontal lines at the bottom and top extremes of the notched regions, respectively, thus completing trapezoidal areas. The rectangular areas below and above these lines represent the data between the 10th and 25th percentile, and the 75th and 90th percentile, respectively. The lower "whisker," below the lower rectangular area, represents the data between the 5th percentile and 10th percentile. Data samples shown by dots below the whisker represent the outlying 5%, including the minimum. The upper whisker, above the upper

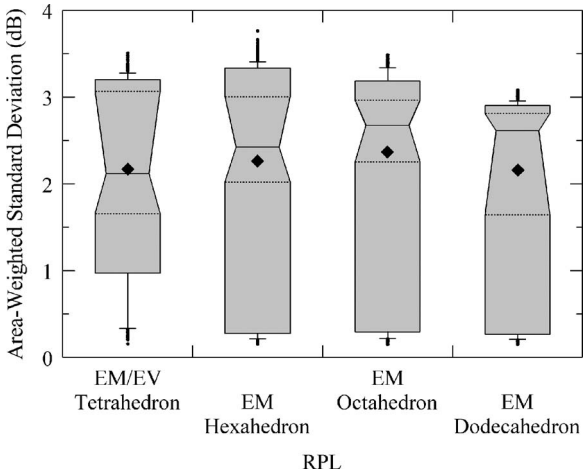

FIG. 11. Notched box-whisker diagrams showing the distribution and grouping of frequency-dependent spatial standard deviation values for the EM RPLs from 100 Hz to 11.2 kHz (through the 8 kHz octave band).

rectangular area, represents the data between the 90th percentile and 95th percentile. Data samples beyond this whisker represent the outlying 5%, including the maximum. The mean value from Table IV is indicated in the diagram by a closed black diamond.

As a general rule, lower values of the diagram indicators suggest superior omnidirectional behavior. For example, lower maximum, minimum, first quartile, third quartile, median, and mean values all suggest better performance, but in different ways. A lower maximum value indicates lower maximum directivity at any frequency. As discussed earlier, a lower mean value may suggest that a RPL is more omnidirectional, but one must still observe the spread in data values and other statistical properties to form an adequate judgment of its actual omnidirectional performance. A lower mean with a large box or whisker spread could clearly be less desirable than a slightly higher mean with a very small spread. A smaller notched box indicates greater uniformity in directivity over much of the bandwidth, but does not necessarily suggest acceptable omnidirectionality. A source that is perfectly omnidirectional at all frequencies would consistently show zero box and whisker spread, no outliers, and zero median and mean values.

By comparing the box-whisker diagrams in Fig. 10, one would likely conclude that the EM/EV tetrahedron is the most omnidirectional EM RPL over the 4 kHz bandwidth, since it produces the lowest maximum, median, and mean values, as well as the smallest box spread. However, one also finds that its first quartile is higher than that of any other EM RPL. The EM dodecahedron would likely be chosen as the second-best performing RPL. Depending upon the selection criteria, either the EM hexahedron or EM octahedron would probably be ranked as the worst performing over the bandwidth. The octahedron produces the highest median and mean values, but the hexahedron produces the highest maximum value and largest upper whisker spread.

Figure 11 demonstrates that the EM dodecahedron produces the lowest mean, upper quartile, and maximum values over the 8 kHz bandwidth, but the EM/EV tetrahedron again produces the lowest median and smallest box spread. Nevertheless, because the 10th and 75th percentile values of the tetrahedron are relatively high, one would likely choose the dodecahedron as the best source over this bandwidth and the tetrahedron as the second best. Once again, either the EM hexahedron or octahedron would likely be chosen as the worst-performing RPL, depending upon the selection criteria.

Using a similar approach for the EV RPLs, the EM/EV tetrahedron would be chosen as the best-performing EV RPL over both the 4 and 8 kHz bandwidths. Over the 4 kHz bandwidth, one would likely choose the EV hexahedron as the second-best performer and either the EV octahedron or EV dodecahedron as the worst performer. The EV icosahedron would probably be chosen as the third-best performer. Over the 8 kHz bandwidth, either the hexahedron or icosahedron could be chosen as the second-best performer, most likely followed by the dodecahedron, then the octahedron.

3. Additional metrics

Other approaches to the data reduction problem might involve the computation of "omnidirectionality coefficients." While such work is beyond the scope of the present paper, a few possibilities are worth mentioning.

A frequency-dependent spatial autocorrelation of radiated energy is one intriguing example that stems from recent analysis of diffusing surfaces[13,14,16,17] and the analogy already mentioned between these surfaces and omnidirectional sources. A single-number figure of merit might also be derived for RPLs in a fashion similar to that suggested by D'Antonio and Cox[15,18] (also see Ref. 13). This would involve computation of the spectral standard deviation of the frequency-dependent spatial standard deviation to show the degree of variation about the spatial standard deviation mean. This single-number standard deviation would then be added to the mean to form the figure of merit.

As in other areas of acoustics, one must exercise caution in producing or using single-number or multiple-number figures of merit if the data reduction robs the data of its interpretive value. A compromise between excessive detail and excessive reduction must be made to ensure that necessary detail is not sacrificed for the sake of simplicity alone.

V. SUMMARY AND CONCLUSIONS

While dodecahedron loudspeakers are currently the most widely used "omnidirectional" sources for room acoustics measurements, they should not necessarily be viewed as more omnidirectional than other RPLs. This is especially true when their directivities are considered over complete measurement bandwidths. The omnidirectional cutoff frequency of a dodecahedron loudspeaker may be higher than that of another RPL with an equal midradius, but all RPLs should be recognized as "multidirectional" sources with varying degrees of directivity above their cutoff frequencies. Since these frequencies often occur near 1 kHz (well within common measurement bandwidths), understanding and comparison of higher-frequency directional behaviors becomes crucial.

Area-weighted spatial standard deviations of 2664 frequency response function levels over a free-field measurement sphere provided more information about omnidirectional performance than gliding-average directional deviations that are implemented using single-plane measurement arcs. The standard deviation method is supported by visual balloon plot observations. It provides an effective global view of source radiation using either narrowband or proportional-band analysis.

This method revealed that a constructed tetrahedron loudspeaker produced better average radiation uniformity than a dodecahedron loudspeaker (or any other constructed RPL) over specified measurement bandwidths. This was true even though its omnidirectional cutoff frequency was the lowest. While no RPL stood out as being consistently exceptional above its cutoff frequency, the tetrahedron was found to produce the most uniform radiation in the 4 kHz octave band. The dodecahedron was also a good choice over the measurement bandwidths, but not simply because it pro-

duced the highest omnidirectional cutoff frequency. The hexahedron produced a cutoff frequency above that of the octahedron, suggesting that its cutoff frequency was better than expected (based on its polyhedron order). The standard deviation method also confirmed that RPLs with smaller midradii consistently produced higher cutoff frequencies than similarly shaped RPLs with larger midradii and volumes. However, attempts to decrease cutoff frequencies through smaller enclosure volumes should be carefully weighed so as to avoid degradation of sound power output, low-frequency output, and spectral uniformity.

Because it was difficult to rank overall omnidirectional performance from the fluctuating frequency-dependent standard deviation curves, notched box-whisker diagrams were introduced as a means of summarizing the directivity information they contained. Octave-band standard deviation curves were also assessed for data reduction and compared to curves from the ISO 3382 source qualification method. The two approaches agreed on some omnidirectional characteristics and rankings, but significantly disagreed on others.

The findings of this paper are based on a limited number of source embodiments. One should therefore use caution in generalizing them to other source geometries, dimensions, loudspeaker driver diameters, etc. Additional theoretical, numerical, and experimental work is needed to further generalize the results and develop needed predictive tools. In particular, greater clarification is required to establish the interconnected roles of individual driver directivities, driver spacings, driver orientations, enclosure diffraction effects, and multiple-driver interference effects in the production of composite RPL directivity patterns. Nevertheless, the findings of this work do provide an experimental basis for future work, while enhancing understanding of RPLs as measurement tools for room acoustics and other applications. They emphasize that the omnidirectional quality of a source should not be judged exclusively by its omnidirectional cutoff frequency or by the satisfaction of relaxed omnidirectional requirements at higher frequencies of interest. They motivate the possibility of using lower-order polyhedra than the dodecahedron with fewer drivers and lower cost as equally viable sources for current standards. While the sound power output of these sources would be smaller for a given type of loudspeaker driver, alternate drivers could be selected as a means of compensation.

The work has demonstrated a viable alternative for assessing source omnidirectionality that is complementary or preferable to current methods. As a result, standardized omnidirectional source qualification methods may benefit from pertinent review and modification. In the future, we recommend that they be approached in a fashion that encourages omnidirectional source designers to significantly improve source omnidirectionality at higher frequencies of interest, rather than merely satisfy the status quo of relaxed requirements. One aim for designers would be to decrease the spatial standard deviation of radiated fields above cutoff frequencies. However, a further-reaching aim would be to significantly increase omnidirectional cutoff frequencies so that sources maintain nearly ideal omnidirectional radiation (as opposed to multidirectional radiation) throughout common measurement bandwidths.

An improvement to the measurement methods described in this paper would involve an increase in the spatial resolution of frequency response measurements over an entire measurement sphere, so that lobing structures at frequencies within the 8 kHz octave band (or higher bands) can be better resolved. While manufacturers should be willing and able to provide such comprehensive high-resolution testing of omnidirectional sources, they and others may also be interested in simplified measurement schemes for occasional rapid testing. To this end, we recommend that the effectiveness of the standard deviation method be investigated for single-plane measurement arcs in addition to complete measurement spheres.

An intriguing aspect of the standard deviation method is its close parallel to established methods of assessing scattering uniformity from diffusing surfaces. The analogies should be further investigated. Related metrics such as "omnidirectionality coefficients" could be developed to better characterize omnidirectional sources for comparative purposes. We encourage research in these areas to improve the evaluation and development of better omnidirectional sources for use in acoustical applications.

ACKNOWLEDGMENTS

This work was funded in part by the Research Experiences for Undergraduates (REU) program of the National Science Foundation (NSF). The authors also acknowledge Gordon Dix, Kent Gee, Todd Kitchen, Wesley Lifferth, and Jacob Robinson for their assistance in the construction of the experimental RPLs and measurement apparatuses, and in the development of numerical analysis tools. They further acknowledge William Christensen for his helpful comments on statistical matters and Viggo Tarnow for encouragement and information regarding his early efforts in omnidirectional source characterization.

[1]"Acoustics—measurement of sound insulation in buildings and of building elements—part IV: field measurements of airborne sound insulation between rooms," ISO 140-4:1998(E), International Organization for Standardization, Geneva, Switzerland, 1998.
[2]H. S. M. Coxeter, *Regular Polytopes*, 2nd ed. (Macmillan, New York, 1963).
[3]V. Tarnow, "Computation of sound radiation from loudspeaker systems with the symmetry of the platonic solids," Proceedings of the Eighth International Congress on Acoustics, London, 1974, p. 617.
[4]V. Tarnow, "Sound radiation from loudspeaker system with the symmetry of the platonic solids," Brüel & Kjær Technical Review **4–1974**, 23–31 (1974).
[5]I. B. Witew and G. K. Behler, "Low-mid frequency measurement of single number parameters in room acoustics with multi-way dodecahedron speakers," Proceedings of Internoise 2005, the 2005 Congress and Exposition on Noise Control Engineering, Rio de Janeiro, Brazil, 2005.
[6]"Acoustics—measurement of the reverberation time of rooms with reference to other acoustical parameters," ISO 3382:1997(E), International Organization for Standardization, Geneva, Switzerland, 1997.
[7]*CRC Standard Mathematical Tables and Formulae*, 29th ed., edited by W. H. Beyer (CRC Press, Boca Raton, FL, 1991), p. 110.
[8]H. M. Cundy and A. P. Rollett, *Mathematical Models*, 3rd ed. (Tarquin, Norfolk, UK, 1961), pp. 84–88.
[9]"Specification for octave-band and fractional-octave-band analog and digital filters," ANSI S1.11-1986, American National Standards Institute, Washington, DC, 1986.

[10]M. R. Schroeder, "Binaural dissimilarity and optimum ceilings for concert halls: More lateral sound diffusion," J. Acoust. Soc. Am. **65**, 958–963 (1979).
[11]P. D'Antonio, "Performance evaluation of optimized diffusors," J. Acoust. Soc. Am. **97**, 2937–2941 (1995).
[12]T. J. Cox, "Designing curved diffusers for performance spaces," J. Audio Eng. Soc. **44**, 354–364 (1996).
[13]T. J. Hargreaves, "Acoustic diffusion and scattering coefficients for room surfaces," Ph.D. thesis, University of Salford, Salford, UK, 2000.
[14]T. J. Hargreaves, T. J. Cox, Y. W. Lam, and P. D'Antonio, "Surface diffusion coefficients for room acoustics: Free-field measures," J. Acoust. Soc. Am. **108**, 1710–1720 (2000).
[15]T. J. Cox, "The optimization of profiled diffusers," J. Acoust. Soc. Am. **97**, 2928–2936 (1995).
[16]T. J. Cox and P. D'Antonio, *Acoustic Absorbers and Diffusers: Theory, Design, and Application* (Spon, London, 2004).
[17]"AES information document for room acoustics and sound reinforcement systems—Characterization and measurement of surface scattering uniformity," AES-4id-2001, Audio Engineering Society, New York, 2001.
[18]P. D'Antonio and T. Cox, "Two decades of sound diffusor design and development. 2. Prediction, measurement, and characterization," J. Audio Eng. Soc. **46**, 1075–1091 (1998).